Chemistry & Biology
Article

Structural Basis for Stabilization of the Tau Pre-mRNA Splicing Regulatory Element by Novantrone (Mitoxantrone)

Suxin Zheng,[1] Yu Chen,[1] Christine P. Donahue,[3] Michael S. Wolfe,[3] and Gabriele Varani[1,2,*]
[1]Department of Chemistry
[2]Department of Biochemistry
University of Washington, Seattle, WA 98195, USA
[3]Center for Neurologic Diseases, Brigham and Women's Hospital and Harvard Medical School, Boston, MA 02115, USA
*Correspondence: varani@chem.washington.edu
DOI 10.1016/j.chembiol.2009.03.009

SUMMARY

Some familial neurodegenerative diseases are associated with mutations that destabilize a putative stem-loop structure within an intronic region of the tau pre-messenger RNA (mRNA) and alter the production of tau protein isoforms by alternative splicing. Because stabilization of the stem loop reverses the splicing pattern associated with neurodegeneration, small molecules that stabilize this stem loop would provide new ways to dissect the mechanism of neurodegeneration and treat tauopathies. The anticancer drug mitoxantrone was recently identified in a high throughput screen to stabilize the tau pre-mRNA stem loop. Here we report the solution structure of the tau mRNA-mitoxantrone complex, validated by the structure-activity relationship of existing mitoxantrone analogs. The structure describes the molecular basis for their interaction with RNA and provides a rational basis to optimize the activity of this new class of RNA-binding molecules.

INTRODUCTION

The microtubule-associated protein tau is expressed predominantly in neurons where it promotes microtubule assembly, reduces microtubule instability, and plays a role in maintaining neuronal integrity and axonal transport (Hirokawa, 1994). Neurofibrillary lesions composed of this protein constitute a defining neuropathological feature of Alzheimer's disease (Spillantini and Goedert, 1998). Filamentous tau protein deposits are also found in other neurodegenerative diseases, many of which are frontotemporal dementias or movement disorders that have been subsumed under the heading of "Pick complex" (Kertesz and Munoz, 1998; Spillantini and Goedert, 1998). Such neurodegenerative disorders associated with tau protein are referred to as tauopathies (Lee et al., 2001). The tau gene consists of 16 exons that are alternatively spliced to generate six major tau isoforms in a developmentally regulated manner (Andreadis et al., 1992; Goedert et al., 1989). They differ from each other by the presence or absence of 29 or 58 amino acid inserts located in the amino-terminal half of the protein and a 31 amino acid repeat located in the carboxy-terminal half. Inclusion or exclusion of the latter by alternative splicing of exon 10 produces tau isoforms with either three (when exon 10 is missing) or four (when exon 10 is present) microtubule-binding repeats (Goode and Feinstein, 1994; Gustke et al., 1994); these isoforms are known as 3R and 4R tau, respectively (Goedert et al., 1989). In the normal adult human brain, the relative ratio of 4R to 3R tau is generally close to unity; overproduction of 4R tau appears to be sufficient to lead to dementia.

Mutations in the tau gene cause familial frontotemporal dementia and parkinsonism linked to chromosome 17 (Clark et al., 1998; Dumanchin et al., 1998; Goedert et al., 1999; Hutton et al., 1998; Morris et al., 1999; Poorkaj et al., 1998; Spillantini et al., 1998). Tau mutations within coding regions cluster in the microtubule-binding repeats and alter the ability of tau to interact with microtubules. This occurrence initiates an unclear set of events that lead to the formation of tau filaments in the neurons of patients affected with a variety of neurodegenerative diseases (Dayanandan et al., 1999; Hasegawa et al., 1998; Hong et al., 1998). However, other mutations causing these diseases are located within introns or are synonymous and cluster near the splice-donor site of the intron following exon 10. Significantly, four mutations at positions +3, +13, +14, and +16 of the intron (with the first nucleotide of the splice-donor site taken as +1; Figure 1A) (Goedert et al., 1999; Hutton et al., 1998; Morris et al., 1999; Spillantini et al., 1998) are found within a putative RNA stem loop that partially masks the splice donor itself. The surprising discovery of these mutations led to the suggestion that the stability of the RNA stem loop affects alternative splicing of exon 10 and that the destabilization of the stem loop itself alters the balance between different tau isoforms and ultimately leads to neurodegeneration in patients carrying mutations within this RNA structure (Hutton et al., 1998).

Several studies demonstrated that the intronic mutations found in frontotemporal dementia and parkinsonism decrease the thermodynamic stability of the RNA stem loop in vitro (Donahue et al., 2006; Hutton et al., 1998; Varani et al., 1999). It was thus postulated that destabilization of this RNA structure partially unmasks the splice site, leading to increase inclusion of exon 10 and therefore to increased production of the 4R tau isoform compared to the 3R isoform (Hutton et al., 1998). More recently, Donahue et al. (2006) have demonstrated the reverse phenomenon as

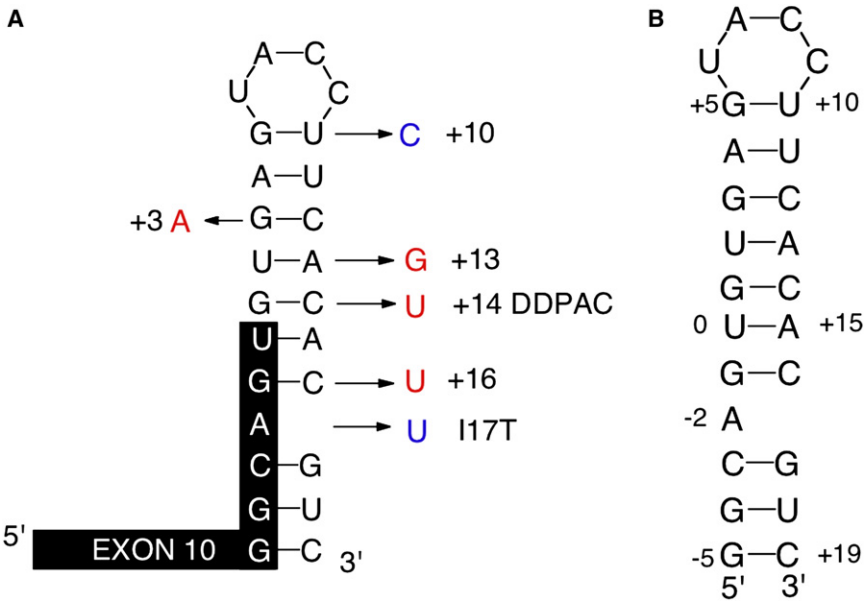

Figure 1. Sequences of Wild-Type and Mutant Tau SREs

(A) Sequences and secondary structures of wild-type and mutant human tau exon 10 SREs. Destabilizing mutations at the +3, +13, +14, and +16 (in red) positions is linked to familial neurodegenerative diseases and increases inclusion of exon 10 (Goedert et al., 1999; Hutton et al., 1998; Morris et al., 1999; Spillantini et al., 1998). In contrast, stabilizing mutations at +10 and the I17T insertion (in blue) decreases inclusion of exon 10 in vitro (Donahue et al., 2006).

(B) The sequence of the wild-type tau SRE containing nucleotides G−5 to C+19 used in our NMR structural studies.

well; namely, mutations that stabilize the RNA stem loop in vitro substantially decrease exon 10 inclusion (and therefore alter the 4R/3R ratio) in an otherwise wild-type tau minigene. Evidence supporting the formation of the tau splicing regulatory element (SRE) stem-loop structure in vivo was provided by the anticorrelation between the stability of the stem loop and the efficiency of antisense inhibition of exon 10 inclusion (Donahue et al., 2006). These experimental findings and the resulting model suggest that small molecules that stabilize the tau SRE RNA stem loop would provide very useful tools to probe the mechanism of neurodegeneration and perhaps new therapeutic avenues to treat these diseases.

The aminoglycoside antibiotic neomycin, a naturally-occurring RNA-binding molecule, was found to bind the tau SRE RNA major groove and to stabilize the RNA structure (Varani et al., 2000). However, this class of molecules lacks the selectivity that would be necessary for therapeutic or even investigative applications. A high-throughput screening assay for compounds that bind to and stabilize the tau SRE RNA identified the anticancer drug mitoxantrone (MTX) from a library of ~110,000 molecules (Figure 2A) (denoted by code number LDN-13978 in Donahue et al. [2007] and revealed as MTX for the first time here) (Donahue et al., 2007). MTX is used in clinical practice as a drug against breast cancer, acute leukemia, and non-Hodgkin's lymphoma (Hagemeister et al., 2005; Tsavaris et al., 2005); it has also been approved in the U.S. for the treatment of patients with progressive multiple sclerosis (Gonsette, 2003). The lead-like activity of MTX in binding to the tau SRE (EC_{50} of ~700 nM) and its current multiple uses in clinical practice makes it an attractive lead to discover new small molecule regulators of tau messenger RNA (mRNA) splicing, but its activity must first be improved.

Here we report the nuclear magnetic resonance (NMR) structure of the complex between MTX and the region of SRE that constitutes the defining structural characteristic of this RNA. MTX intercalates into the partially open bulge region of tau SRE RNA with the side chains forming sequence-specific hydrogen bonds with the nearby RNA bases and electrostatic interactions with the phosphate backbone. The structure explains the structure-activity relationship (SAR) of a series of MTX analogs and provides the structural basis for the design of more potent and specific regulators of tau pre-mRNA splicing.

RESULTS

Formation and Stoichiometry of the MTX-Tau RNA Complex

In order to characterize the MTX-RNA complex, we titrated tau SRE RNA with MTX at concentrations suitable for NMR investigations (0.1–1 mM) and recorded spectra for the imino proton region, where the RNA resonances corresponding to Watson-Crick paired nucleotides are well resolved (Figure 2B). From the bottom, the spectra correspond to MTX/RNA ratios of 0.0, 0.5, 1.0, 1.5, 2.0, and 3.0. The chemical shifts of the imino resonances in the upper helical region (G+1, U+2, and G+3) were not changed, but only broadened during the titration. For resonances near the bulge loop (G−1 and U0), we observed a decrease in the intensity of the peak corresponding to the free RNA signal as the MTX concentration increases; at the same time, a new set of peaks appeared at distinct positions that were later assigned to the MTX-bound form of the RNA. The peaks corresponding to the free form of the RNA disappear completely only when the ratio of MTX/RNA is >2.0 (Figure 2B). Multiple sets of imino resonances appear when the ratio of MTX/RNA is larger than 1.5; these new peaks must arise from the binding of multiple copies of MTX to the RNA when more than one molecule of MTX per RNA is present. The observation of distinct peaks in slow exchange on the NMR time scale corresponding to free and bound RNA indicates that MTX binds tightly (K_d < 1 μM) at or near the RNA bulge region, which is consistent with an EC_{50} of about 700 nM previously reported (Donahue et al., 2007).

The observation of two peaks with comparable intensity corresponding to the free and bound RNA resonances at MTX/RNA ratios of about 1 (see, e.g., U0; Figure 2B) has two possible explanations. MTX could bind as a dimer or it could form more

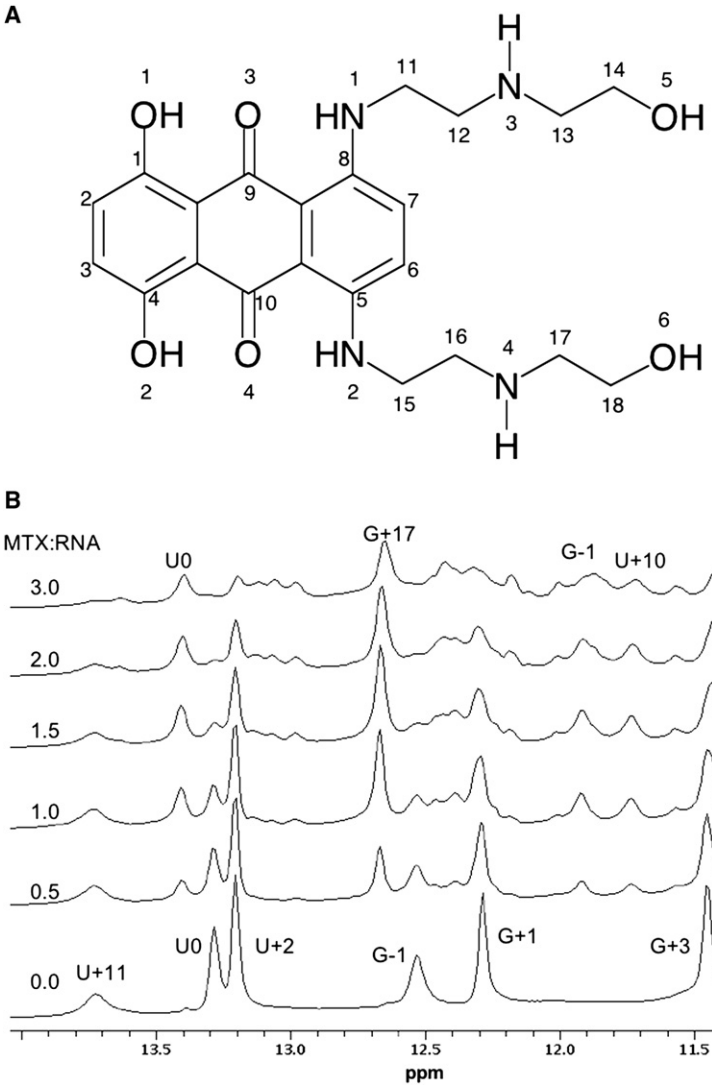

Figure 2. Structure of MTX and Spectra of NMR titration of Tau SRE RNA

(A) Structure of MTX.

(B) NMR titration of tau SRE RNA with increasing concentrations of MTX recorded at 4°C. From the bottom, spectra correspond to the following ratios of MTX/RNA: 0.0, 0.5, 1.0, 1.5, 2.0, and 3.0. The label in the bottom spectrum corresponds to the assignments for the free RNA, whereas the top label corresponds to the MTX-bound RNA.

than one independent interaction with the RNA. The observation of additional peaks in the 1D spectra at ratios above 1:1 strongly suggests that when there are two binding sites, an additional MTX molecule binds with comparable affinity to a second site within the RNA. On the other hand, the reported self-association constant (12400 ± 4000 L mol^{-1}) of MTX in aqueous solutions (Davies et al., 2001) and the 1D titration experiment show that MTX should be dimeric at NMR concentrations.

We confirmed the dimeric form of free MTX in solution by observing intermolecular nuclear Overhauser effects (NOEs) between the H2/3 resonances of one MTX and the H6/7 resonances as well as the side chain resonances (H11/15 and H12/16) of a second copy of the molecule (Davies et al., 2001). These NOE interactions are only possible if the two MTX molecules are arranged in a reversed stacking conformation sitting on each other in a head-to-tail orientation. However, in the 2D NOESY spectra of the complex, we failed to observe any intermolecular NOEs involving two MTX molecules between the H2/3 and H6/7 of MTXs; we also failed to observe NOEs between the H2/3 aromatic resonances and the same side chain resonances (H11/15 and H12/16) that were observed instead for free MTX. All these NOEs would be expected for a dimeric structure and indeed were observed for the free MTX dimer. As a control, we readily observed NOEs between the H6/7 resonances and the side chain H11/15 and H12/16 in the RNA complex; in fact, these NOEs were much stronger compared to the free MTX dimeric structure, most likely because the conformation of the side chain is rigidified in the complex (see below), leading to more efficient NOE transfer. If MTX bound to RNA as a dimer, we would expect to see much stronger NOEs than we observe in the RNA-free MTX dimer between the aromatic H2/3 and H6/7, as well as the side chain H11/15 and H12/16 resonances. Altogether, these results are inconsistent with the binding of MTX as an antiparallel dimer to the tau SRE RNA. Although it is possible that MTX dimerizes, forming a parallel stacking arrangement (in this case, intra- and intermolecular NOEs would be very difficult to distinguish), this is highly unlikely because of the resulting electrostatic repulsion. Thus, the titration experiments are better explained by a model where multiple molecules of MTX bind to different locations on the RNA.

Consistent with the conclusion that two MTX molecules bind to the SRE RNA in distinct locations, we observed two distinct sets of intermolecular NOEs when analyzing NOESY spectra. A more numerous and more intense set of intermolecular contacts mapped to the RNA bulge; a second, much less numerous, set corresponded to the minor groove near the upper helix. Binding of MTX to the minor groove of the RNA does not lead to significant chemical shift changes in the RNA, suggesting that this interaction is only superficial and perhaps corresponds to the nonspecific electrostatic interactions between the highly cationic MTX and the negatively charged phosphate backbone.

The binding sites of MTX on tau SRE RNA was mapped by chemical shift perturbation analysis as well (see Tables S1 and S2 available online). Modest chemical shift changes were observed in the upper stem loop, never larger than 0.12 ppm, where the NOE data indicate that a second molecule of MTX binds. Much more significant chemical shift changes were

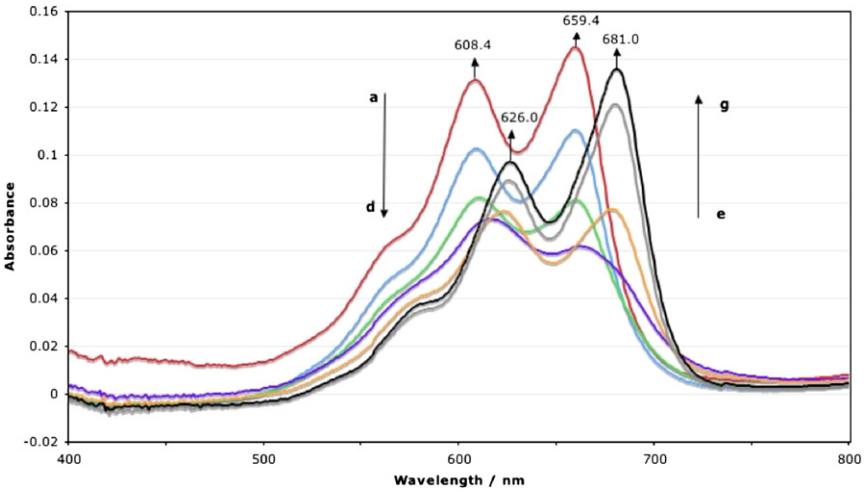

Figure 3. Titration of Tau SRE RNA with MTX Monitored by UV/Vis Spectroscopy

The experiments were carried out in buffer solution (10 mM; pH 6.0) containing 10 μM MTX in the presence of different RNA concentrations. RNA/MTX are as follows: 0.0 (a); 0.02 (b); 0.05 (c); 0.1 (d); 0.2 (e); 0.5 (f); 1.0 (g). The absorbance was saturated after the ratio of RNA/MTX reached 1.0.

observed near the bulge region (A−2). The chemical shift change for the H8 of A−2 is 0.16 ppm; the imino resonance of G+17 was not observed in the free form due to exchange with solvent, but readily observed in the complex with MTX. The largest chemical shift change is observed for the imino of G−1 (0.62 ppm). The observation of the G+17 imino in the complex, but not in the free form, indicates that this resonance is shielded from solvent in the complex either because the bulge region is stabilized by the binding of MTX, because MTX itself shields this hydrogen, or both. Thus, all available NMR results are consistent with the conclusion that MTX binds to tau SRE RNA in two locations. A first site corresponds to the region near the bulge; binding of MTX here induces significant chemical shift changes, indicating an intimate interaction, and is likely responsible for the stabilization of the stem loop. A second complex forms in the minor groove close to the upper helical region; this second complex does not induce large conformational and chemical shift changes in the RNA.

To further establish the physical chemical characteristics of the anthraquinone chromophore in the complex, we used UV/Vis and fluorescence spectroscopy. The experiment differs from the NMR titration because RNA is now titrated into a fixed amount of MTX (10 μM) and not the reverse. The maxima in absorbance of free MTX were located at 608.4 and 659.4 nm (Figure 3). In the first stage of the titration (RNA/MTX < 0.1), the intensities of these two absorbance peaks decreased sharply; in the second stage, the intensities of the two new peaks (626 and 681 nm; Figure 3) increased gradually until saturation was reached at an RNA/MTX ratio ≥1.0. Both absorption peaks shift to the red by about 18 and 22 nm, respectively; such bathochromic effects are commonly observed for DNA intercalators (Li et al., 2005). Comparable bathochromic effects were also observed in fluorescence titration experiments (Figure S1). The UV/Vis and fluorescence data indicates that MTX binds to tau SRE RNA by partially intercalating or at least forming clear stacking interaction with base ring systems. The two-stage binding mode (first, the free MTX intensity decrease quickly; second, the bound MTX absorption increases gradually) suggests that there are multiple MTX binding sites. The sharp initial decrease in absorbance may be due to RNA condensation caused by charge interactions when multiple MTX molecules, each with two positive charges, bind to one RNA molecule and neutralize the negative charges in the phosphate backbone (Kapuscinski and Darzynkiewicz, 1984, 1986). In the second stage, as the titration continues, MTX molecules redistribute among increasing amounts of available free RNAs, until eventually most find their preferred binding sites are saturated.

The NMR results indicate that there are multiple binding sites for MTX on the RNA. Sharp NMR spectra were obtained at MTX/RNA ratios near 1.0. Under this condition, we observed two sets of resonances near the lower bulge corresponding to the free and bound forms of the RNA, with comparable intensities. Despite the increased complexity in the spectra at 1:1 ratio, the signals corresponding to bound and free components can be distinguished unambiguously at high field (Figures S3 and S4), particularly when using partially deuterated nucleotides or $^{13}C/^{15}N$-labeled RNA in 3D spectra. Increasing the MTX/RNA ratio (e.g., at ratios of 1.5:1 and 2:1) to saturate binding at the bulge caused considerable broadening in the aromatic and ribose regions of the NMR spectrum, presumably due to conformational exchange involving the other weaker sites (e.g., the site near the apical loop). Furthermore, there are not sufficient intermolecular NOEs to define the minor groove binding conformation. Thus, we chose the 1:1 ratio as the best condition to determine the structure of the complex; under these conditions, we could only study the most favorable and specific binding site on tau SRE near the bulge immediately adjacent to the splice junction.

NMR Spectral Assignments

Spectral assignments were obtained in a straightforward manner starting from the available assignments for the free RNA (Figure S2). Some assignments were obtained by observing exchange peaks near the diagonal, others simply by following the conventional procedures that connected both the free and bound RNA peaks (in the MTX binding site) to a single set of peaks corresponding to resonances that do not shift in the complex (Figures S3 and S4). Assignments are reported in Table S1. Critical to structure determination was the observation of intermolecular NOEs between the MTX side chains and RNA resonances; some are shown in the 2D NOESY spectrum of Figure 4A; their complete list is reported in Table S4. At 25°C, we observed numerous intermolecular NOEs between MTX side chains and the RNA, but none was observed with the MTX ring H2/3 resonances. As a result, the location of the

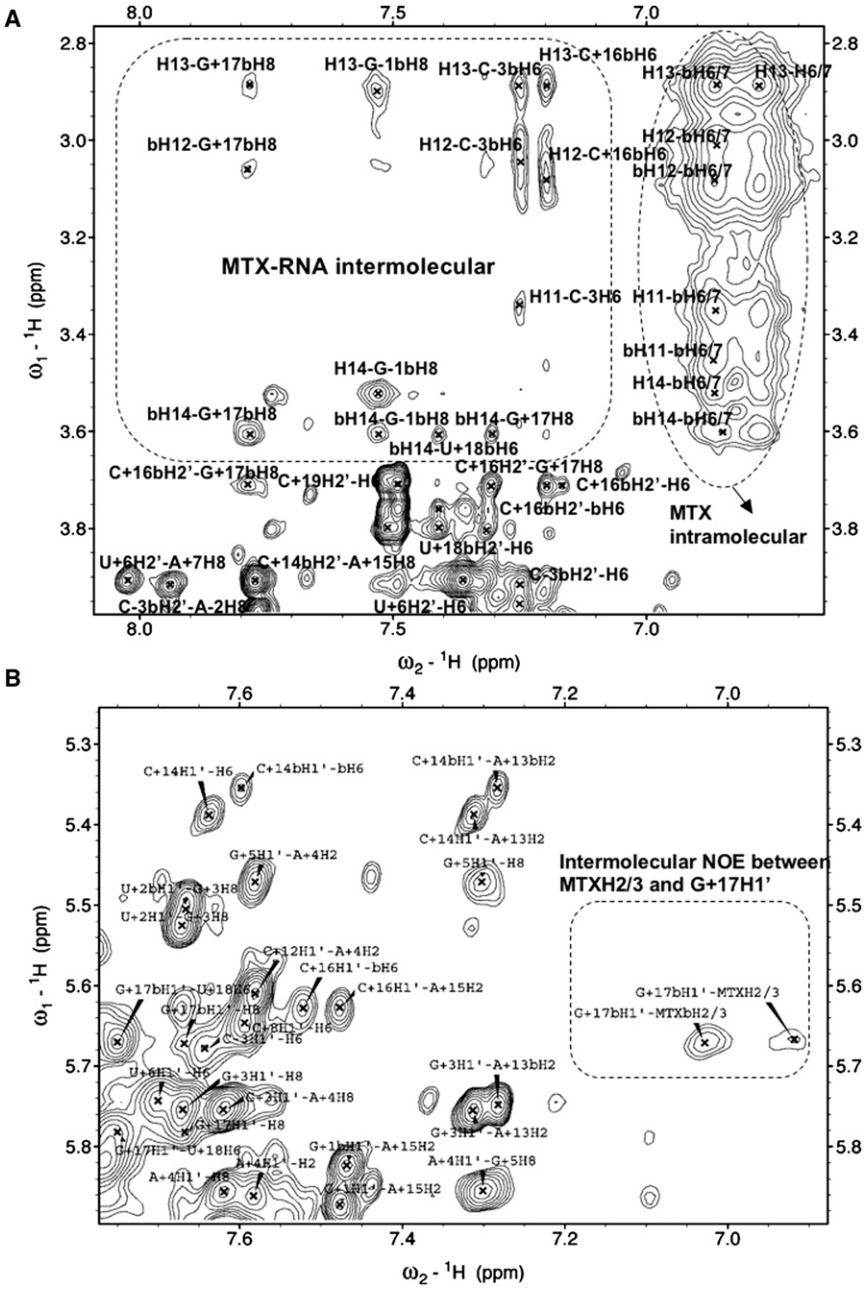

Figure 4. Two-Dimensional NOESY Experiment Recorded at 4°C on the Complex between MTX and Tau SRE RNA

(A) Regions of the spectrum corresponding to intra- (MTX) and intermolecular (MTX and RNA) NOEs are boxed and labeled.

(B) The intermolecular NOE observed for G+17H1' and MTXH2/3. "b" refers to the bound component. For example, H13-G+17bH8 refers to the NOE between the MTXH13 and the G+17-bound H8.

anthraquinone chromophore relative to the RNA could not at first be defined unambiguously.

The data at 25°C are consistent both with the chromophore being inserted into the bulge region and stacked on the RNA bases and with the chromophore pointing away from the bulge region with only the MTX side chains interacting with the RNA. We deemed this second conformation unrealistic because of the results of the UV/VIS experiments that suggest partial intercalative binding and because it would expose the hydrophobic chromophore to solvent. However, we sought to establish the correctness of the first conformation unambiguously. Although the peaks become broader at lower temperature, the NOESY spectra could still be assigned at 4°C with the help of partially deuterated RNA (that decreases the linewidth due to less efficient relaxation) and of $^{13}C/^{15}N$-labeled RNA. At 4°C, we observed key intermolecular NOEs between MTX H2/3 and the H1' of G+17 (Figure 4B), which indicates that MTX was stacked on the base of G+17, consistent with the most likely of the two conformations described above.

Structure of the Complex between MTX and Tau SRE RNA

Structure calculations were carried out using NIH-Xplor and standard protocols (Clore and Kuszewski, 2003) using a total of 41 intermolecular NOEs (Table S4). From 100 calculated structures, the top 20 were chosen to represent the ensemble of conformations based on their energy and restraint violation statistics. Statistics of data collection and for the converged structure are shown in Table 1. The superposition of the ten best structures (Figure 5A) shows the helical stem and bulge where MTX binds are very well defined, but the apical loop remains conformationally flexible. The anthraquinone chromophore of MTX stacks on the base of G+17, consistent with the large chemical shift change for its NH, while the positively charged side chains interact with the major groove of the RNA; the unpaired A−2 nucleotide protrudes outward into solution (Figure 5B). The length and helical axis of the RNA in the complex were almost unaltered compared to the free RNA structure (Varani et al., 1999).

Close-up views of the interaction between MTX and RNA taken from the best-scoring structure are shown in Figure 5C. Consistent with the UV/VIS results and the protection of the G+17 imino from exchange with solvent, the chromophore of MTX is stacked between the base pairs of G+17–C−3 and C+16–G−1, forming partial stacking interaction with both base pairs. This interaction may be the dominant driving force for the formation of the complex. In addition, a well ordered network of hydrogen bonds and electrostatic contacts is observed between the MTX side chains and tau SRE RNA. The distances

Table 1. Experimental Constraints and Structure Statistics

Experimental constraints	
RNA-RNA distance constraints	516
RNA-MTX distance constraints	41
Hydrogen-bonding constraints	51
Base-pair planarity restraints	18
Dihedral constraints	173
Dipolar couplings	30
Total experimental constraints	829
Average RMS deviations from experimental restraints[a]	
Distance	0.04 Å
Dihedral	0.85°
RDC	0.53 Hz
Average RMS deviations from ideal geometries[a]	
Bonds	0.0034 Å
Angles	0.78°
Impropers	0.40°
RMS deviation from average structure[a] (heavy atom)	
Full structure	2.33 ± 0.61 Å
Double helical stem (G−1–A+4; U+11–C+16)	0.77 ± 0.40 Å
MTX binding site (G−4–U0; A+15–U+18)	1.02 ± 0.43 Å
MTX	0.74 ± 0.32 Å

Standard deviation is used for the error bars.
[a] The top 20 out of 100 calculated structures were selected as converged structures.

of all relevant hydrogen-bonding and electrostatic contacts are shown in Table S5. These additional interactions increase both the affinity of MTX binding and presumably the stability of the tau SRE RNA structure (Donahue et al., 2007). Although the predicted pKa (http://ibmlc2.chem.uga.edu/sparc/) showed that the two amines (N3 and N4) should be protonated at the experimental pH (pH ~6), we did not include any specific electrostatic term during structure calculation or refinement to avoid introducing any unintended bias in the structure determination process. Thus, the additional electrostatic and hydrogen-bonding interactions observed in the complex, such as the electrostatic interaction between N4 of MTX and phosphate of G+17 and hydrogen bond between O6 of MTX and O4 of U+18 (Figure 5C), are derived from the experimental intermolecular NOE constraints (Table S4), although not directly verified from experimental data (such as RNA-MTX scalar couplings).

In the complex, the N3 and N4 amines in the MTX side chains form hydrogen bonds with the O6 of the G−1 and N7 of G+17 bases, respectively (Figure 5C). The MTX N4 amine can form hydrogen bonds with the base of G+17 and at the same time electrostatic contacts with the phosphate of G+17. One hydroxyl group (O6) of MTX is in hydrogen-bonding contact with the O4 of U+18, while another hydroxyl group (O5) is hydrogen bonded with the phosphate of G−1. Although the hydrogen bond between the imino N2 group and the phosphate of C+16 is not likely to provide specificity for a particular RNA sequence, the hydrogen bond between the imino group N1 and O6 of G−1 is specific for the G−1 base. The two hydroxyl groups in the chromophore can also form hydrogen bonds with the O2' of C+16 and A−2, as supported by weak NOE interaction with A−2, providing selectivity over DNA and a distinct mode of binding. Although the intercalation of the anthraquinone chromophore into RNA is not believed to be sequence specific, the hydrogen bonds between the side chain N3/4 of MTX and the G−1 and G+17 bases can provide specificity for adjacent GC base pairs in a structural context permissive to binding, as generated by the bulged A−2 nucleotide.

SAR for MTX Analogs

To explore the SAR of MTX binding to tau SRE RNA, a series of MTX analogs (Table 2) were obtained from the National Cancer Institute and tested for their ability to stabilize the tau RNA stem loop, using a fluorescence resonance energy transfer assay that uses a tau RNA oligonucleotide with a fluorophore on the 3′ end and a quencher on the 5′ end of the stem loop (Donahue et al., 2007). Satisfactorily, the NMR structure of the complex is for the most part consistent with the results of Table 2. In the structure, the hydrophilic groups of MTX (O1/2, O5/6, and N3/4) are involved in a well defined hydrogen-bonding network, as described above. All observable activity is eliminated when these hydrophilic groups are substituted with nonpolar groups (compound **4** in Table 2). The N3/4 amine groups form hydrogen bonds with the guanine bases from the two GC base pairs abetting the unpaired A−2 nucleotide. Even a change in the N3/4 amine to ether groups, as in **1**, leads to a >70-fold decrease in the EC_{50}. The O1/2 hydroxyl groups involved in hydrogen bonds with the hydroxyl O2′ of C+16 and A−2 contribute less to RNA binding, because their substitution to hydrogen only reduces the EC_{50} about six times (**3**). To our surprise, modifying the O5/6 hydroxyl groups to the better hydrogen-bonding donor amines (**2**) did not increase binding, but instead decreased the EC_{50} more than 7000 times.

DISCUSSION

Modulating RNA with small molecule drugs would provide the opportunity to regulate the function of RNA in chronic and infectious disease conditions (Thomas and Hergenrother, 2008). An inviting target for small molecules that bind to RNA is the SRE within the tau pre-mRNA that controls the ratio of the two major tau protein isoforms. Mutations that destabilize the tau stem-loop structure increase inclusion of exon 10 and are associated with neurodegenerative tauopathies. Since mutations that stabilize the RNA can reduce exon 10 inclusion, stabilization of the stem loop with a small molecule would also reduce exon 10 inclusion. Thus, if we were able to regulate alternative splicing of tau exon 10, we would be better able to define its precise role in a variety of neurodegenerative disease conditions and perhaps explore new therapeutic options as well.

Unfortunately, there is no precedent for the successful clinical or even preclinical development of RNA-binding small molecules outside of the ribosome, a mainstay target of antibacterial treatment. Among well known antibacterials targeting the ribosome are aminoglycoside antibiotics such as neomycin. In a previous study, we showed that this drug binds in the major groove of the tau SRE RNA. However, these molecules have poor specificity and are synthetically challenging; they have been proven to be unattractive leads to the development of new RNA-binding drugs because of the lack of selectivity that would be necessary

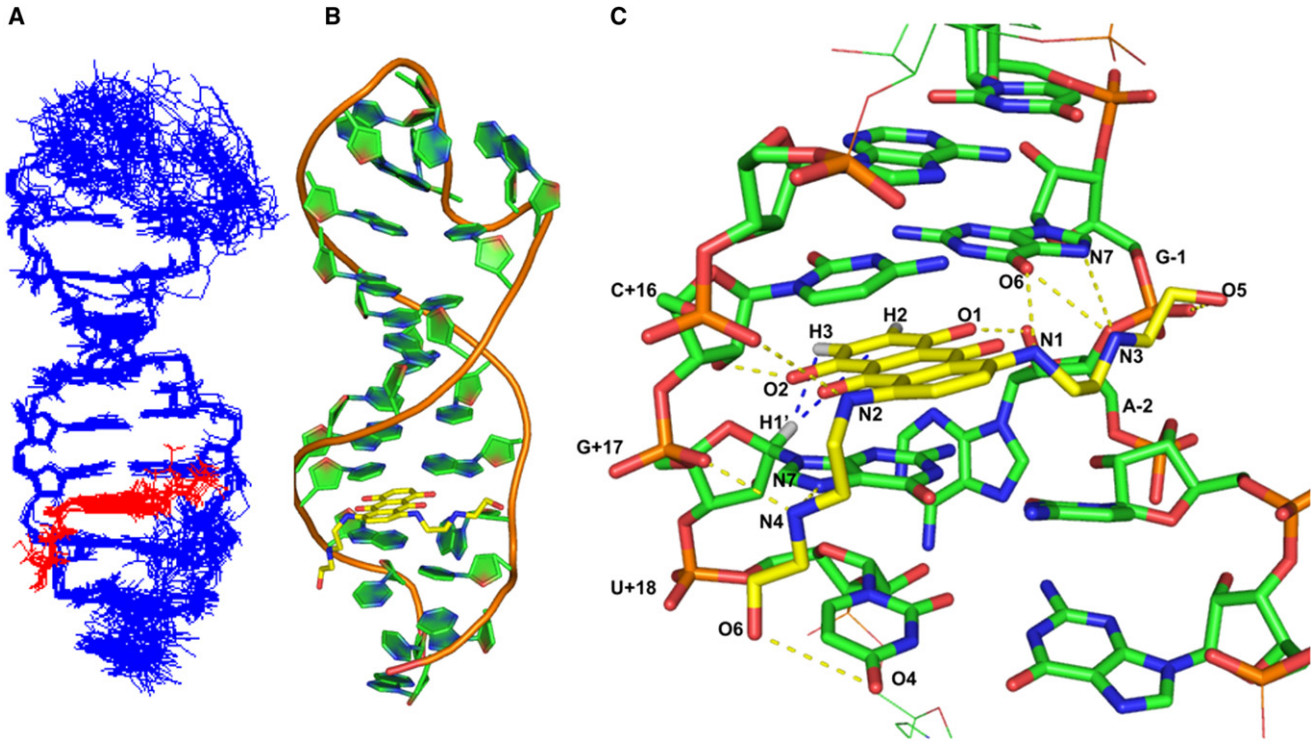

Figure 5. Structure of the Tau SRE RNA-MTX Complex

(A) Superposition of the ten best calculated structures (heavy atoms only) represented with MOLMOL (Koradi et al., 1996). The RNA is shown in blue and MTX is shown in red.

(B) The best calculated structure. MTX is shown in yellow stick representation and the RNA backbone is shown in brown with Pymol (DeLano, 2002).

(C) Close-up view of the tau SRE RNA-MTX interaction. The carbon atoms of MTX are shown in yellow and the RNA in green with Pymol (DeLano, 2002); some key intermolecular NOEs between the H1' of G+17 and H2/3 of MTX are shown by blue dashed lines.

for therapeutic efficacy. In the search for new small molecules that interfere with tau pre-mRNA splicing, the anticancer drug MTX was found to bind to the tau SRE and stabilize its structure in a screen of over 100,000 molecules (Donahue et al., 2007). Here we report the structure of its complex with tau SRE RNA and a molecular rationale for its binding activity.

The activity of MTX as an anticancer drug has led to some interest in understanding the molecular basis of its interaction with DNA, but so far these studies have been based on molecular modeling (Islam et al., 1985; Kostjukov et al., 2007) and not a formal structure. In addition to providing a structural basis to further optimizing the affinity and specificity of MTX for tau pre-mRNA stem-loop structure, the present structure also sheds more insight into the general mechanism of the interaction of MTX with nucleic acids in general.

MTX binds the bulge region of tau SRE RNA by partially intercalating in the space created by the extruded base A−2 and by forming hydrogen bonds to two adjacent GC base pairs (G−1–C+16 and G+17–C−3) and one uracil residue (U+18) nearby that are specific to these bases. Although free MTX self-associates, forming a dimer, a variety of spectroscopic observations indicate that MTX binds to tau SRE RNA as a monomer and has a second, slightly weaker binding site in the minor groove of the RNA near the apical stem loop. The second binding site is most probably due to superficial electrostatic interactions between the positively charged MTX and the RNA backbone, because chemical shift changes in the RNA upon binding are very small. In contrast to the main complex near the bulge, we cannot establish this second binding conformation due to the paucity of intermolecular NOEs observed for it.

Table 2. SAR for MTX Analogs

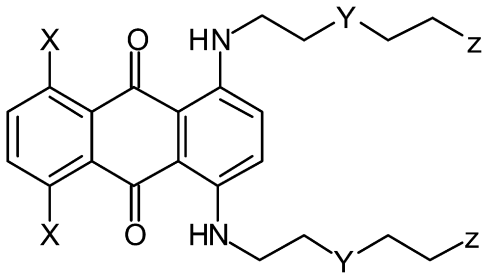

Compound	X	Y	Z	EC_{50} (μM)
MTX	OH	NH	OH	0.72
1	OH	O	OH	>50
2	OH	NH	NH2	>5000
3	H	NH	OH	4.3
4	H	CH2	CH3	NA

The partial intercalation of the chromophore and electrostatic contacts with the RNA do not lead to sequence-specific binding, but require nonetheless a specific structure, a bulged nucleotide. Moreover, the hydrogen bonds between the MTX side chain amine N3/4 and the base O6 carbonyls of G−1 and N7 of G+17 suggest that MTX prefers to recognize GC base pairs (G−1–C+16 and C−3–G+17). Although these interactions are clearly sequence specific, the flexibility of the side chains allows the positions of the hydrogen-bonding groups to adapt themselves to other RNA sequences and bind to them with comparable effectiveness. However, the structure suggests that by rigidifying these amines in a more constrained structure, it should be possible to optimize hydrogen-bonding interactions between MTX and the GC base pairs and thereby generate MTX derivatives that are specific for the tau SRE structure.

In addition to the side chain amines, the hydroxyl group O6 of MTX is in hydrogen-bonding contact with the O4 of U+18, a result well established by one of the strongest intermolecular NOEs observed between the H18 of MTX and the H5 of U+18. This hydrogen-bonding interaction also contributes to the specific recognition of U+18. Therefore, the length of the MTX side chain between O6 and the chromophore may be varied to enforce stronger hydrogen bonds with U+18 to select against other RNAs. We plan to exploit these suggestions in future studies to improve the binding characteristics of MTX derivatives with the tau stem loop and to generate MTX variants that selectively bind to this structure.

SIGNIFICANCE

Modulating RNA structure with small molecule drugs would provide the opportunity to regulate the function of RNA in chronic and infectious disease conditions. An inviting target for small molecules that bind to RNA is the SRE within the tau pre-mRNA that controls the ratio of the two major tau protein isoforms. Mutations that destabilize the tau SRE RNA increase inclusion of exon 10 into the mature tau protein and are associated with neurodegenerative tauopathies. Since mutations that stabilize the RNA reduce exon 10 inclusion, stabilization of the stem loop with small molecules would also reduce exon 10 inclusion and provide a new way to define its precise role in a variety of neurodegenerative disease conditions and to explore new therapeutic options. The anticancer drug MTX was recently identified in a high-throughput screen to stabilize the tau SRE RNA. Here, we report the structure of tau pre-mRNA in complex with MTX at the bulge region, which identifies a new class of RNA-small molecule interactions. This structure provides a basis to optimize the potency and specificity of MTX analogs and sheds light into the general mechanism of the interaction of MTX with nucleic acids.

EXPERIMENTAL PROCEDURES

RNA Preparation

A model oligonucleotide mimic of the wild-type tau SRE containing nucleotides from G−5 to C+19 (Figure 1B) was used in all experiments. RNA oligonucleotides were synthesized by in vitro transcription using T7 polymerase and synthetic DNA templates (IDT) with commercially available unlabeled, selectively deuterated, and $^{13}C/^{15}N$-labeled nucleotides (Cambridge Isotope Inc.). The selectively deuterated nucleotides were used to simplify the NMR spectra by only containing H2/H6/H8 and H1′/2″ resonances; all other positions were deuterated. All RNA samples were purified as described (Price et al., 1998). Microdialysis was used to bring the final buffer to 10 mM sodium-phosphate (pH 6.0) with 0.1 mM EDTA. Lyophilized RNAs were redissolved in 5% D_2O/95% H_2O or 100% D_2O as needed. Samples used for residual dipolar coupling (RDC) measurements were mixed with Pf1 phage (ASLA Ltd) and dialyzed against the same buffer at a final phage concentration of 12–15 mg/ml. MTX (>97%) was purchased from Sigma and used without further purification.

Data Collection and Analysis

Most NMR data were acquired on Bruker 500 MHz and 600 MHz Avance spectrometers equipped with cryoprobes and a 750 MHz DMX spectrometer equipped with a conventional HCN probe. The D_2O NOESY on the complex was collected at Pacific Northwest National Laboratory on a Varian 800 MHz spectrometer equipped with a cryoprobe. In-Phase-Anti-Phase HSQC spectra (Andersson et al., 1998) for RDC measurements were collected at 500 MHz. Data were processed with nmrPipe (Delaglio et al., 1995) and analyzed with Sparky (Goddard and Kneller, 2008). The spectra for the H_2O sample were recorded at 4°C and those for the spectra in D_2O were recorded both at 25°C and 4°C.

The assignments for the complex were initiated by standard 2D NOESY walks that were extended from the part of the structure that did not change upon binding to MTX into the section where changes were observed (see also Figures S2 and S3); the assignments were facilitated by 3D NOESY-HSQC experiments due to the fact that ^{13}C shifts did not change considerably upon MTX binding (Varani et al., 1996). The bound resonances were further confirmed by observing exchange peaks in 2D NOESY spectra (Figure S3); the partial deuterated sample was used to reduce the overlap in the ribose region (Figure S4). The complete proton assignments of free and bound tau SRE RNA are listed in Table S1 and the assignments of MTX are listed in Table S3. Base pairs were established from the imino peaks observed in 2D water NOESY collected with Watergate water suppression (Dingley and Grzesiek, 1998; Pervushin et al., 1998). Dihedral angle restraints were obtained from 2D TOCSY experiments, as described (Varani et al., 1996), and the C2′-*endo* constraints for the sugar pucker were used only when both H1'/H2' and H1'/H3' coupling were large.

Structure Calculations

NOEs involving nonexchangeable protons were classified as strong (1.8–3.2 Å), medium (2.2–4.2 Å), weak (2.5–5.5 Å), or very weak (3.0–7.0 Å) based on cross-peak intensities at 100 and 200 ms mixing times (2D NOESY experiments) and 120 ms (3D NOESY-HSQC). NOEs involving exchangeable protons were characterized as strong (1.8–3.4 Å), medium (1.8–4.5 Å), weak (1.8–6.0 Å), and very weak (1.8–6.5 Å) based on their NOE cross-peak intensities at 100 and 200 ms mixing times (Chen et al., 2006).

A single extended starting structure was generated with Xplor-NIH (Schwieters et al., 2003) and the structure calculations were carried out by Xplor-NIH with the same strategy by using the means of conformational database potential (Clore and Kuszewski, 2003). RDC-derived restraints were added only after the majority of converged structures were found and only RDCs obtained from well ordered residues devoid of conformational exchange were used in refinement (Leeper and Varani, 2005).

Optical Spectroscopy Studies

UV/Vis absorbance spectra were obtained on a Beckman DU-650 spectrophotometer equipped with a quartz micro-colorimetric vessel of 1 cm path length.

Activity Measurement of MTX Analogs

MTX analogs were obtained from the National Cancer Institute and were tested for their ability to stabilize the tau RNA stem-loop structure using a fluorescence resonance energy transfer assay as previously described (Donahue et al., 2007) in which the 5′ end of the tau RNA oligomer is linked to dabsyl and the 3′ end is linked to fluorescein.

ACCESSION NUMBERS

Coordinates have been deposited in Protein Data Bank with accession code 2kgp.

SUPPLEMENTAL DATA

Supplemental Data contain four figures and five tables and can be found with this article online at http://www.cell.com/chemistry-biology/supplemental/S1074-5521(09)00112-4.

ACKNOWLEDGMENTS

We thank the Environmental Molecular Sciences Laboratory-Pacific Northwest National Laboratory (PNNL) for access to NMR instruments and Nancy Isern (PNNL) for help with data acquisition; Thomas Leeper for assistance with the NMR spectroscopy; Zahra Shajani, Mi-Kyung Lee, and Amy Davidson for help with RNA preparation; Michael F. Bardaro for help with RDC data collection; and Lev Elson-Schwab for the help with fluorescent data collection. This work was supported in part by grants from the National Institutes of Health.

Received: December 10, 2008
Revised: February 20, 2009
Accepted: March 11, 2009
Published: May 28, 2009

REFERENCES

Andersson, P., Nordstrand, K., Sunnerhagen, M., Liepinsh, E., Turovskis, I., and Otting, G. (1998). Heteronuclear correlation experiments for the determination of one-bond coupling constants. J. Biomol. NMR *11*, 445–450.

Andreadis, A., Brown, W.M., and Kosik, K.S. (1992). Structure and novel exons of the human tau gene. Biochemistry *31*, 10626–10633.

Chen, Y., Fender, J., Legassie, J.D., Jarstfer, M.B., Bryan, T.M., and Varani, G. (2006). Structure of stem-loop IV of Tetrahymena telomerase RNA. EMBO J. *25*, 3156–3166.

Clark, L.N., Poorkaj, P., Wszolek, Z., Geschwind, D.H., Nasreddine, Z.S., Miller, B., Li, D., Payami, H., Awert, F., Markopoulou, K., et al. (1998). Pathogenic implications of mutations in the tau gene in pallido-ponto-nigral degeneration and related neurodegenerative disorders linked to chromosome 17. Proc. Natl. Acad. Sci. USA *95*, 13103–13107.

Clore, G.M., and Kuszewski, J. (2003). Improving the accuracy of NMR structures of RNA by means of conformational database potentials of mean force as assessed by complete dipolar coupling cross-validation. J. Am. Chem. Soc. *125*, 1518–1525.

Davies, D.B., Veselkov, D.A., Evstigneev, M.P., and Veselkov, A.N. (2001). Self-association of the antitumour agent novatrone (mitoxantrone) and its hetero-association with caffeine. J. Chem. Soc. [Perkin 2] 61–67.

Dayanandan, R., Van Slegtenhorst, M., Mack, T.G.A., Ko, L., Yen, S.H., Leroy, K., Brion, J.P., Anderton, B.H., Hutton, M., and Lovestone, S. (1999). Mutations in tau reduce its microtubule binding properties in intact cells and affect its phosphorylation. FEBS Lett. *446*, 228–232.

Delaglio, F., Grzesiek, S., Vuister, G.W., Zhu, G., Pfeifer, J., and Bax, A. (1995). NMRPipe: a multidimensional spectral processing system based on UNIX pipes. J. Biomol. NMR *6*, 277–293.

DeLano, W.L. (2002). The PyMOL Molecular Graphics System (http://www.pymol.org).

Dingley, A.J., and Grzesiek, S. (1998). Direct observation of hydrogen bonds in nucleic acid base pairs by internucleotide $^{2}J_{NN}$ couplings. J. Am. Chem. Soc. *120*, 8293–8297.

Donahue, C.P., Muratore, C., Wu, J.Y., Kosik, K.S., and Wolfe, M.S. (2006). Stabilization of the tau exon 10 stem loop alters pre-mRNA splicing. J. Biol. Chem. *281*, 23302–23306.

Donahue, C.P., Ni, J., Rozners, E., Glicksman, M.A., and Wolfe, M.S. (2007). Identification of tau stem loop RNA stabilizers. J. Biomol. Screen *12*, 789–799.

Dumanchin, C., Camuzat, A., Campion, D., Verpillat, P., Hannequin, D., Dubois, B., Saugier-Veber, P., Martin, C., Penet, C., Charbonnier, F., et al. (1998). Segregation of a missense mutation in the microtubule-associated protein tau gene with familial frontotemporal dementia and parkinsonism. Hum. Mol. Genet. *7*, 1825–1829.

Goddard, T.D., and Kneller, D.G. (2008). SPARKY 3. (http://www.cgl.ucsf.edu/home/sparky/).

Goedert, M., Spillantini, M.G., Jakes, R., Rutherford, D., and Crowther, R.A. (1989). Multiple isoforms of human microtubule-associated protein tau: sequences and localization in neurofibrillary tangles of Alzheimer's disease. Neuron *3*, 519–526.

Goedert, M., Spillantini, M.G., Crowther, R.A., Chen, S.G., Parchi, P., Tabaton, M., Lanska, D.J., Markesbery, W.R., Wilhelmsen, K.C., Dickson, D.W., et al. (1999). Tau gene mutation in familial progressive subcortical gliosis. Nat. Med. *5*, 454–457.

Gonsette, R.E. (2003). Mitoxantrone in progressive multiple sclerosis: when and how to treat? J. Neurol. Sci. *206*, 203–208.

Goode, B.L., and Feinstein, S.C. (1994). Identification of a novel microtubule binding and assembly domain in the developmentally regulated inter-repeat region of tau. J. Cell Biol. *124*, 769–782.

Gustke, N., Trinczek, B., Biernat, J., Mandelkow, E.M., and Mandelkow, E. (1994). Domains of tau protein and interactions with microtubules. Biochemistry *33*, 9511–9522.

Hagemeister, F., Cabanillas, F., Coleman, M., Gregory, S.A., and Zinzani, P.L. (2005). The role of mitoxantrone in the treatment of indolent lymphomas. Oncologist *10*, 150–159.

Hasegawa, M., Smith, M.J., and Goedert, M. (1998). Tau proteins with FTDP-17 mutations have a reduced ability to promote microtubule assembly. FEBS Lett. *437*, 207–210.

Hirokawa, N. (1994). Microtubule organization and dynamics dependent on microtubule-associated proteins. Curr. Opin. Cell Biol. *6*, 74–81.

Hong, M., Zhukareva, V., Vogelsberg-Ragaglia, V., Wszolek, Z., Reed, L., Miller, B.I., Geschwind, D.H., Bird, T.D., McKeel, D., Goate, A., et al. (1998). Mutation-specific functional impairments in distinct tau isoforms of hereditary FTDP-17. Science *282*, 1914–1917.

Hutton, M., Lendon, C.L., Rizzu, P., Baker, M., Froelich, S., Houlden, H., Pickering-Brown, S., Chakraverty, S., Isaacs, A., Grover, A., et al. (1998). Association of missense and 5′-splice-site mutations in tau with the inherited dementia FTDP-17. Nature *393*, 702–705.

Islam, S.A., Neidle, S., Gandecha, B.M., Partridge, M., Patterson, L.H., and Brown, J.R. (1985). Comparative computer graphics and solution studies of the DNA interaction of substituted anthraquinones based on doxorubicin and mitoxantrone. J. Med. Chem. *28*, 857–864.

Kapuscinski, J., and Darzynkiewicz, Z. (1984). Condensation of nucleic acids by intercalating aromatic cations. Proc. Natl. Acad. Sci. USA *81*, 7368–7372.

Kapuscinski, J., and Darzynkiewicz, Z. (1986). Relationship between the pharmacological activity of antitumor drugs Ametantrone and mitoxantrone (Novatrone) and their ability to condense nucleic acids. Proc. Natl. Acad. Sci. USA *83*, 6302–6306.

Kertesz, A., and Munoz, D. (1998). Pick's disease, frontotemporal dementia, and Pick complex: emerging concepts. Arch. Neurol. *55*, 302–304.

Koradi, R., Billeter, M., and Wüthrich, K. (1996). MOLMOL: a program for display and analysis of macromolecular structures. J. Mol. Graph. *14*, 51–55.

Kostjukov, V.V., Pahomov, V.I., Andrejuk, D.D., Davies, D.B., and Evstigneev, M.P. (2007). Investigation of the complexation of the anti-cancer drug novantrone with the hairpin structure of the deoxyheptanucleotide 5′-d(GpCpGpApApGpC). J. Mol. Struct. *843*, 78–86.

Lee, V.M.Y., Goedert, M., and Trojanowski, J.Q. (2001). Neurodegenerative tauopathies. Annu. Rev. Neurosci. *24*, 1121–1159.

Leeper, T.C., and Varani, G. (2005). The structure of an enzyme-activating fragment of human telomerase RNA. RNA *11*, 394–403.

Li, N., Ma, Y., Yang, C., Guo, L., and Yang, X. (2005). Interaction of anticancer drug mitoxantrone with DNA analyzed by electrochemical and spectroscopic methods. Biophys. Chem. *116*, 199–205.

Morris, H.R., Perez-Tur, J., Janssen, J.C., Brown, J., Lees, A.J., Wood, N.W., Hardy, J., Hutton, M., and Rossor, M.N. (1999). Mutation in the *tau* exon 10 splice site region in familial frontotemporal dementia. Ann. Neurol. *45*, 270–271.

Pervushin, K., Ono, A., Fernández, C., Szyperski, T., Kainosho, M., and Wüthrich, K. (1998). NMR scalar couplings across Watson-Crick base pair hydrogen bonds in DNA observed by transverse relaxation-optimized spectroscopy. Proc. Natl. Acad. Sci. USA *95*, 14147–14151.

Poorkaj, P., Bird, T.D., Wijsman, E., Nemens, E., Garruto, R.M., Anderson, L., Andreadis, A., Wiederholt, W.C., Raskind, M., and Schellenberg, G.D. (1998). Tau is a candidate gene for chromosome 17 frontotemporal dementia. Ann. Neurol. *43*, 815–825.

Price, S.R., Oubridge, C., Varani, G., and Nagai, K. (1998). Preparation of RNA:protein complexes for X-ray crystallography and NMR (Seattle, WA: Oxford University Press).

Schwieters, C.D., Kuszewski, J.J., Tjandra, N., and Marius Clore, G. (2003). The Xplor-NIH NMR molecular structure determination package. J. Magn. Reson. *160*, 65–73.

Spillantini, M.G., and Goedert, M. (1998). Tau protein pathology in neurodegenerative diseases. Trends Neurosci. *21*, 428–433.

Spillantini, M.G., Murrell, J.R., Goedert, M., Farlow, M.R., Klug, A., and Ghetti, B. (1998). Mutation in the tau gene in familial multiple system tauopathy with presenile dementia. Proc. Natl. Acad. Sci. USA *95*, 7737–7741.

Thomas, J.R., and Hergenrother, P.J. (2008). Targeting RNA with small molecules. Chem. Rev. *108*, 1171–1224.

Tsavaris, N., Kosmas, C., Kavantzas, N., Lazaris, A., Skopelitis, E., Dimitrakopoulos, A., Siakantaris, M., Papalambros, E., Diamantis, N., Patsouris, E., et al. (2005). Breast cancer following curative chemotherapy for non-Hodgkin's lymphoma and the effect of drug resistance proteins to the final outcome. A retrospective study. J. BUON *10*, 71–76.

Varani, G., Aboul-ela, F., and Allain, F.H.T. (1996). NMR investigation of RNA structure. Prog. Nucl. Magn. Reson. Spectrosc. *29*, 51–127.

Varani, L., Hasegawa, M., Spillantini, M.G., Smith, M.J., Murrell, J.R., Ghetti, B., Klug, A., Goedert, M., and Varani, G. (1999). Structure of tau exon 10 splicing regulatory element RNA and destabilization by mutations of frontotemporal dementia and parkinsonism linked to chromosome 17. Proc. Natl. Acad. Sci. USA *96*, 8229–8234.

Varani, L., Spillantini, M.G., Goedert, M., and Varani, G. (2000). Structural basis for recognition of the RNA major groove in the tau exon 10 splicing regulatory element by aminoglycoside antibiotics. Nucleic Acids Res. *28*, 710–719.

